Numerical Modeling of the Lateral Behavior of Concrete-Filled FRP Tube Piles in Sand

Mostafa Jafarian Abyaneh, Hany El Naggar[1], and Pedram Sadeghian

Department of Civil and Resource Engineering, Dalhousie University,
1360 Barrington Street, Halifax, NS, B3H 4R2 Canada.

Abstract

In this study, a numerical model is developed to study concrete-filled FRP tube (CFFT) pile behavior and interactions with foundation soil under lateral loading. The model, based on nonlinear finite element analysis (NFEA) and the disturbed state concept (DSC), considers material and geometrical nonlinearity as well as the interface of soil with fiber-reinforced polymer (FRP). Furthermore, the structural and geotechnical performance of the interface of soil and CFFT pile is studied by utilizing 3D finite element models of full-scale field tests conducted during the construction of a highway bridge on route 40 in Virginia. Based on deflection along the length of the pile, the model results are in good agreement with the experimental data. To investigate the effects of various parameters on the behavior of CFFT piles and local buckling, a parametric study was also performed on different geometrical and material properties, including the pile diameter to length ratio, FRP tube thickness, concrete strength, and soil properties. It was found that the surrounding soil and length to diameter ratio exerted the most noticeable influence, followed by concrete strength. The FRP thickness had the least impact on the results.

DOI: https://doi.org/10.1061/(ASCE)GM.1943-5622.0001725

[1] Corresponding Author: hany.elnaggar@dal.ca

Keywords: Pile, Fiber-reinforced polymer (FRP), Concrete-filled FRP tube (CFFT), Soil-structure interaction, Nonlinear finite element analysis (NFEA), Interface and contact problem.

Introduction

Failure of bridge foundations exposed to corrosion in a marine environment can result in the collapse of the entire structure. The safety and durability of bridge structures thus necessitate long-term maintenance and is of great concern to civil engineers and government departments in the design of sustainable infrastructure. Because the superstructure is dependent upon the foundation, replacing corroded piles can be difficult and expensive (Roddenberry et al. 2014). For this reason, highway agencies and researchers have begun to investigate the use of anti-corrosive materials and the viability of protecting bridge piles with composite materials such as fiber-reinforced polymer (FRP) composites, especially in the form of concrete-filled FRP tube (CFFT) piles (Mirmiran and Shahawy 1997 and Fam et al. 2003b). FRP is a composite material made of a polymer matrix reinforced with fibers. Different types of polymer matrix are often used in the composites, including epoxy, vinyl ester, or polyester resins. FRP tubes used in CFFTs is usually manufactured using filament winding technique, and then the tube is filled with concrete. The advantage of FRPs used in CFFTs with respect to conventional piles casted in steel molds without FRP is that they are less susceptible to corrosion in corrosive and harsh environments. Furthermore, the FRP tube will provide a passive confinement to the concrete core to enhance the strength and ductility of the core. On the other hand, the filling concrete can provide lateral support to the FRP tube to overcome buckling problems (Fam et al. 2003b). Over the last two decades, FRP composite materials were used in practice for several deep foundation applications ranging from bearing piles for light structures to waterfront barriers and fender piles (Fam et al. 2003a; Fam and Rizkalla 2001a; b; Mirmiran and Shahawy 1996, 1997).

Valez and Rayhani (2017) studied the axial and lateral load transfer mechanism of hollow FRP tube piles in soft clay. In this study, the load transfer behavior of small-scale FRP piles was compared to that of traditional steel piles to evaluate the feasibility of FRPs as piling materials. The FRP fiber orientation was found to have a significant influence on the pile capacity. Piles with lower stiffness experienced larger pile head deflections under lateral loading compared to steel piles. A case study was conducted by Pando et al. (2006) on CFFTs used in the foundation of a bridge on Route 40 in Virginia under axial and lateral loadings. By comparing the lateral responses of the CFFT and the reinforced concrete (RC) piles, they showed a similar lateral stiffness up to a lateral load of approximately 40 to 50 kN, which is due to the propagation of cracking in the composite pile. The CFFT pile showed lower stiffness than RC pile in the post-cracking zone while continuing to sustain lateral load with relatively larger deformations.

While pile foundations are mainly subjected to axial loads, in some circumstances, they will be subjected also to lateral loads due to excavation, scouring, seismic loads, or other reasons (Liang et al. 2013a; b; Poulos 2014). Hence, the lateral performance of piles is of great importance, and several researchers have conducted numerous theoretical and experimental studies to investigate this behavior. Chae et al. (2004) conducted experimental and numerical studies on a laterally loaded conventional short piles and pier foundations located near slopes by using a three-dimensional finite-element model (FEM). The piles were assumed to be linearly elastic, whereas the sand was considered to have non-associative properties by using the Mohr-Coulomb (MC) failure criterion. Based on the concept of the subgrade reaction theory, Zhang et al. (2013) proposed semi-analytical solutions using the power-series method to evaluate the response of a vertical pile with different cross sections and embedded in a multilayered soil system to support lateral loads at the head level. The solution was verified by back-predicting responses of laterally-

loaded concrete piles in two existing cases. By comparing results, it was noticed that the pile response was controlled by the subgrade soil stiffness at shallow depth of nearly 3–4 times the pile diameter. This finding was found to hold in this study also as discussed later.

Su and Zhou (2015) determined the effects of the loading direction on the behavior of laterally loaded pile groups by using a comprehensive experimental study. Pile groups with various configurations embedded in sand were subjected to lateral loads along different horizontal directions. The results show that the loading direction has a predominant effect on the evolution and eventual distribution of force among piles in the pile group, the bending responses along the piles, and the total lateral resistance of the pile group. Han et al. (2017) used an energy-based semi-analytical approach to study the performance of pile foundations under lateral loading conditions. Based on the results, a stiffer pile response is observed when degrees of freedom in certain directions are constrained in the soil. Hazzar et al. (2017) performed a three-dimensional numerical study to evaluate the effects of vertical loads on the behavior of laterally loaded piles. The piles were modeled as linear elastic materials in elastoplastic soil using the Mohr-Coulomb constitutive model with a non-associated flow rule. Numerical results showed that the lateral resistance of the pile did not vary considerably with vertical loads in a homogeneous sandy soil. On the other hand, applying vertical loads on a pile embedded in clayey soil was discovered to be detrimental to its lateral capacity.

Although many studies have been conducted on the structural behavior of CFFTs, the soil-structure interaction of CFFT piles was not previously considered. It is important to consider the interaction of CFFTs and soil, since the behavior of underground piles is more complex than that of conventional columns. In the present research, a nonlinear finite element model is developed to predict the mechanical behavior of CFFT piles embedded in soil. The damage model and failure

criterion used in the proposed model are based on the disturbed state concept (DSC) and the Mohr-Coulomb failure criterion, respectively. To verify the computational results, experimental data from precast CFFT piles used in the construction of a new bridge on route 40 in Virginia (Pando et al. 2006) were used to obtain the model parameters for different lateral loadings. After verification of the developed model, a parametric study was carried out to determine the effects of the specimen length to diameter ratio, FRP tube thickness, concrete strength, and surrounding soil on the lateral deflection, FRP axial tensile stress at the extreme tension fiber, soil pressures, bending moment, shear force, and axial load of the pile.

Numerical Modeling

The two main structural components of CFFT piles are the concrete infill and the FRP tube. The relative stiffness of these two components controls the pile performance in relation to vertical and lateral loads. A numerical model based on the DSC damage model and the Mohr-Coulomb failure criterion is developed to predict the elastic-plastic behavior of CFFT piles under various lateral loading conditions, by using nonlinear finite element analysis (NFEA) in three dimensions. The interface of composite piles with the confining soil is also investigated in the proposed model.

Disturbed State Concept

The proposed model is based on the DSC damage model, in which, the behavior of the material can be expressed in terms of the behaviors of its components during deformation (Desai, 2015). The DSC model is formulated as the decomposition of the material behavior into relatively intact (RI) component representing the undamaged behavior of the material, and a fully adjusted (FA) component representing the microcracked part of the material. A schematic representation of the

DSC damage model is shown in Fig. 1, where the white and black areas represent the RI and FA components, respectively. In its initial response, all of the material is relatively intact (RI), without any cracks or microcracks. As the applied loading increases, the FA response becomes more predominant, and the propagation of microcracks results in entirely FA behavior at failure. Between the two extremes of the material state (i.e., between RI and FA), the disturbance factor, according to the concept proposed by Desai (2001), can be represented as:

$$D = D_u(1 - e^{-A\zeta_D^Z}) \tag{1}$$

where D_u is the ultimate value of the disturbance, and A and Z are material parameters, and ζ_D is the accumulated deviatoric plastic strain:

$$\zeta_D = \sum_{n=1}^{nstp} (dE_{ij}^p dE_{ij}^p)^{\frac{1}{2}},\ i, j = 1, 2, 3 \tag{2}$$

where i are j are the tensor index notations corresponding to the three Cartesian directions x, y, and z (1,2 and 3 in the above equation), E_{ij} is the deviatoric strain tensor of the total strain tensor ε_{ij} and the integral is from first loading step (n=1) up to last loading step (n_{stp}). The disturbance of two arbitrary points in the plastic zone can be found by using the following equation and substituting in Eq. 1 to determine the A and Z parameters of Eq. 1 above.

$$D = \frac{\sigma^{RI} - \sigma}{\sigma^{RI} - \sigma^{FA}} \tag{3}$$

where σ^{RI}, σ^{FA} and σ represent relatively intact (RI), fully adjusted (FA), and the current stresses, respectively. In the modeling procedure, the RI and FA states are correlated as a function of the deviatoric plastic strain. As shown in the graph in Fig. 1, the disturbance increases as the microcracks propagate in the element.

The three parameters D_u, A, and Z are the disturbance parameters used to predict the mechanical behavior of the corresponding material from experimental or field tests. The residual strength and

confining conditions control the FA behavior, whereas the elastic modulus and Poisson's ratio and cohesion (if existing) affects the RI behavior. Once the disturbance parameters are defined for each element, stress increments can be obtained using the following equation (Desai 2015):

$$d\sigma_{ij} = (1 - D)C^{ep}_{ijkl}d\varepsilon_{kl} + \frac{D}{3}\delta_{ij}C^{ep}_{ppkl}d\varepsilon_{kl} - dD(\sigma^{RI}_{ij} - \sigma^{FA}_{ij}) \quad (4)$$

Where the disturbance value (D) equals zero in the pre-failure stage. Models that can be used to predict the RI response of the material range from simple mathematical models to constitutive models such as the Mohr-Coulomb failure criterion. In this research, the nonlinear finite element analysis (NFEA) was conducted by considering large deformation and adopting the Mohr-Coulomb failure criterion. The results of the model were then used as the RI response of the material using the elastic stiffness matrix C^e, which can be interpreted as relatively undamaged behavior. On the other hand, the residual strength of the material is obtained by considering the FA state as shown in Fig. 1. At the beginning, the material behavior will be in its RI state (i.e., the Gaussian point has not yielded yet). As the loading increases and the behavior starts being nonlinear, governed by an elasto-prefectly plastic behavior (i.e., Gaussian point has yielded), the damage parameter will start increasing from zero to a value, D_u, then the elastoplastic stiffness matrix C^{ep} is corrected for each increment of stress using Eq.4. i.e., upon finding the disturbance (D) in Eq. 1 for two arbitrary points of the graph, the elastoplastic stiffness matrix, C_{ep}, given in Eq. 5 (by Khoei 2005) is then corrected to account for damage caused in the post-peak response, as shown in Eq. 4 to find the stress increments. Then, the current state of stress in the element can be obtained by adding the stress increment given by Eq. 4 to the stress in the element calculated from the previous step.

$$C_{ep} = C_e - \frac{C_e\, n\, n^T C_e}{H + n^T C_e\, n}$$

Where H is the hardening modulus, n is the flow rule vector that represents the growth direction of the failure surface.

The utilized plasticity model (Mohr-Coulomb)

The Mohr-Coulomb failure criterion was used as the plasticity model to govern the material behavior of the solid elements and to consider the interface behavior as well as the effect of friction. The corresponding yield surface is an irregular hexagon in the principal stress space. An important characteristic of this model is that it can provide different elastoplastic stress-strain curves for various paths of stress for different loading conditions such as simple shear, compression, and extension loading. For this reason, the applied plasticity model is often regarded as appropriate for frictional materials. The yield function of the Mohr-Coulomb failure criterion can be written as (Zienkiewicz and Taylor 2005):

$$F = J_1 \sin\phi + \sqrt{J_{2D}}\cos\theta - \frac{\sqrt{J_{2D}}}{3}\sin\phi\,\sin\theta - c\,\cos\phi \tag{6}$$

where J_1 and J_{2D} represent the first invariant of stress, and the second invariant of deviatoric stress, respectively; and c and ϕ represent the cohesion and angle of friction of the Mohr-Coulomb failure criterion. θ is the Lode angle, which can be written as:

$$\theta = \frac{1}{3}\sin^{-1}\left(-\frac{3\sqrt{3}}{2}\frac{J_{3D}}{J_{2D}^{3/2}}\right) \tag{7}$$

where J_{3D} is the third invariant of deviatoric stress. The value of θ must be acquired within the range of $[-\pi/6, \pi/6]$ (Zienkiewicz and Taylor 2005).

The Developed Three-Dimensional Finite Element Model

The mechanical behavior of CFFTs and concrete piles can be predicted by the proposed model. It should be noted that this model can also be used for the CFFT columns, which are a special case

of CFFT piles. The main factors addressed by the model are: (i) the contact problem associated with the interface of concrete, FRP laminate and soil, (ii) large deformations, considered in several increments and iterations, (iii) the modeling of plasticity by using the Mohr-Coulomb failure criterion, and (iv) the softening effect of concrete in compression, based on the disturbed state concept.

A three-dimensional mesh of elements was generated for a cylindrical CFFT pile. A schematic representation of the mesh generated is shown in Fig. 2. It should be noted that the figure is scaled to illustrate the configuration of the elements. Each element was mapped onto a cubic element with unit dimensions as shown for an arbitrary element. For each element, the stresses were calculated for eight quadratic Gaussian points, by using values of $3^{-1/2}$ for the coordinates, with respect to the unit value in each direction (Zienkiewicz and Taylor 2005). After the main calculations were performed, to extract the modeling results, the stress values were extrapolated by the same reverse procedure as for the element nodes. Thus, instead of using a circular sector element, cubic elements with unit dimensions were utilized for the interpolation and extrapolation of stress values.

To address the contact problem resulting from the interface of the composite pile and soil, a separate mesh was generated for concrete, soil and contact elements (see Fig. 3). As can be seen in Fig. 3, the interface of the composite pile and soil is represented by the white areas between the soil and the concrete. Full bonding between the concrete and the FRP tube was assumed since the calculated shear stress was in the range of 35 to 50 kPa, which is much lower than the bond strength between FRP and concrete measured by Helmi et al. (2005) for a similar situation. Moreover, the slippage behavior at the interface of the pile and the soil was modeled by using the Mohr-Coulomb

failure criterion similar to the used plasticity model. It should be noted that the mesh generated was scaled used for a schematic illustration of the mesh.

Local Buckling under Axial Compression and Lateral Soil Pressure

The critical stress for local buckling can be controlled by using the following procedure: An approximate closed-form solution for axial loading can be developed to check the local buckling of the pile. According to Batdorf (1947), for medium-length cylinders, the smallest critical stress can be estimated by using Eq. 8, for a cylinder with a radius of r, and a wall thickness of t:

$$\sigma_{z,cr}=0.577\frac{Et}{r\sqrt{1-\nu^2}} \tag{8}$$

When soil pressure exists, the governing buckling equation can be expressed as:

$$\sigma_{\theta,cr}=\frac{E}{4(1-\nu^2)}\left(\frac{t}{r}\right)^2 \tag{9}$$

The combined pile loading does not result in local buckling if the following formula is satisfied (Odland 1978):

$$C_{z\theta}=\left(\frac{\sigma_z}{\sigma_{z,cr}}\right)^2+\left(\frac{\sigma_\theta}{\sigma_{\theta,cr}}\right)^2\le 1 \tag{10}$$

If the local buckling factor ($C_{z\theta}$) is less than one, it can be concluded that applying both lateral soil pressure and axial loading to a hollow pile will result in a greater probability of buckling than is the case with pure axial compression. Thus, if a hollow pile fails due to buckling at the ground surface, there is a higher chance of buckling at the depth of maximum axial stress.

Model Verification

To verify the parameters of the proposed model, experimental field test results were obtained from Fam et al. (2003b). The composite piles were concrete-filled glass fiber-reinforced polymer

(GFRP) tubes considered for a highway bridge on route 40 in Virginia, with an outer diameter and tube thickness of 624.8 mm (24.6 in.) and 5.41 mm (0.213 in.), respectively. The wall structure of the GFRP tube consisted of three layers. The thickness of the inner and outer layers was each 1.88 mm, and they composed of fibers oriented at ±34 degrees with respect to the axial axis of the tube. The middle layer's thickness was 1.65 mm and contained fibers oriented at 85 degrees with respect to the axial axis. The profile of the surrounding soil at the site was composed of various soil layers, including sand and clay. The soil conditions were loose at the top and stiff at the bottom of the soil layers. In Fig. 4, the cross-section of the concrete pile is presented along with the soil profile, as well as an arbitrary cross-section, A-A. The total length of the composite pile was 13.1 m, including the length of the pile that was not covered by soil. The compressive strength of the concrete used was reported to be 41.4 MPa (Fam et al. 2003b).

Material Properties

Table 1 presents the mechanical properties of soil, concrete, and FRP used in the proposed model: the elastic modulus (E), Poisson's ratio (ν), cohesion (c), and the angle of internal friction (ϕ). The developed model considered three upper Sand layers (Sand 1, Sand 2 and Sand 3), overtopping a deeper clay layer. The parameters used in Table 1 were obtained from the SPT test results reported by Pando et al. (2006) shown in Fig. 4 and using a commonly used soil correlations for strength and stiffness (i.e., Schmertmann, 1975; Kulhawy & Mayne, 1990; Bowles, 1997 and the CFEM 2006). The FRP tube properties presented in Table 1 were also obtained from the same experimental study by Pando et al. (2006) and confirmed by Fam et al. (2003b) and Kaw (2005). In the model, a friction coefficient (μ) of 0.31 was used. The initial modulus of elasticity (E) for concrete is based on the following equation related to the requirements of Committee 318 of the American Concrete Institute (ACI) (2014):

$$E_c = 4700\sqrt{f'_c} \tag{11}$$

where E_c and f'_c represent the elastic modulus and the compressive strength of concrete in MPa, respectively. The parameters of the Mohr-Coulomb failure criterion were obtained by using the following equations (Zhao 2000):

$$\begin{cases} \varphi = \sin^{-1}\left(\dfrac{f'_c - f'_t}{f'_c + f'_t}\right) \\ c = \dfrac{\sqrt{f'_c f'_t}}{2} \end{cases} \tag{12}$$

where f'_t represent the uniaxial tensile strength of concrete, which can be expressed as (ACI committee 318 2014):

$$f'_t = 0.62\sqrt{f'_c} \tag{13}$$

Model Verification Results

Model verification graphs are presented in Fig. 5, showing the lateral deflection for four different lateral loads cycles applied at the top of the composite pile: 48.9, 80.1, 93.5, and 120.1 kN. As shown in the figure, the lateral deflection of the composite pile below a depth of seven meters is approximately zero indicating that the pile is fully fixed in the ground below this depth. Besides, it can be noticed that a slight stiffening occurred in the response between the second and third loading cycle (i.e., between the 80.1 kN and the 93.4 kN). This stiffening may be related to the soil failure that occurred in the top portion of the pile (i.e., in the top 3 meters) as the passive capacity of the soil was exceeded during the second loading cycle whereas the lower part is still not yielded (below - 3 meters). Also, the pile appeared to form a hinge at a depth of about 5 m, as can be noticed, particularly from the performance of the last two load cycles as the surrounding soil started to yield. For example, as the maximum load from the second to the third cycles

increased by approximately 17% the lateral deflection increased by about 17% (i.e., from 16.1 to 18.9 mm), whereas, after the supporting soil yielded, the deflection increased by almost 80 % as the maximum load increased by only 29% between the third and fourth loading cycles. It can be seen from Fig. 5 that there is a good agreement between the developed model predictions and the experimental data, and that the developed model is capable of simulating the pile and soil behaviors adequately. As a result, the developed model can be used to perform parametric studies, as described below.

Parametric Study

The effect of different model parameters including height-to-diameter ratio of specimens, FRP tube thickness, concrete strength and surrounding soil was investigated on the moment, shear, axial curves as well as lateral deflection and FRP and soil stresses of composite piles along the depth under a 100 kN of applied load.

Effect of length/diameter ratio

As shown in Fig. 6, three different length/diameter (L/D) ratios: 15, 20, and 25, were used in the proposed model to investigate the effect of geometry on the lateral deformation of composite piles under a constant lateral load of 100 kN. A constant composite pile length (L) of 13.1 m was assumed, while the diameter (D) was changed in order to compare the results. As can be seen in the figure, the greater the L/D ratio at a certain depth, the greater the lateral deflection of the composite pile.

The proposed model was used to examine the effect of the length/diameter (L/D) ratio of CFFT piles on the bending moment, shear force, axial load, and axial tensile stress of the FRP

tube, and on the lateral deformation plotted against the normalized depth (Z/D). The results of the corresponding parametric study are shown in Fig. 6. It can be seen that an increase in D (i.e., a decrease in L/D) results in an increased maximum moment, shear force and axial load for the CFFT pile. Moreover, the normalized depth at which the maximum moment occurs decreases with lower L/D values. The bending capacity of CFFT piles with a diameter of 0.62 m is reported to be approximately 502 kN.m (Fam and Rizkalla 2001a). Higher shear force and axial load values were obtained for composite piles with lower L/D ratios, as shown in Fig. 6 (e) and (f). In addition, Fig. 6 (b) shows an increase in the FRP axial tensile stress at the extreme tension fiber with a higher L/D ratio, although the trend was not consistent. Stresses exceeding 250 MPa were not considered as zero, due to the brittle mechanical behavior of FRP laminates. In Fig. 6 (a), the effect of L/D values on lateral deflection is depicted. Fig. 6 (c) shows that an increasing L/D ratio also results in greater stresses in the soil.

Effect of FRP tube thickness

To determine the effect of FRP thickness (t) on the mechanical behavior of CFFT piles, different FRP thicknesses, including 5, 7, and 9 mm, were studied. In addition to providing better passive confining pressure for the CFFT piles, a thicker FRP layer also reduces the lateral pile deformation due to the greater strength of the composite material. The maximum lateral CFFT pile deflections obtained at ground level were 28.4 and 27.8 cm, for FRP thicknesses of 9 and 5 mm, respectively. Increasing the thickness of the FRP laminate also resulted in a small increase (1-3%) in the maximum FRP tensile stress, and in the maximum soil compressive stress. Moreover, a five percent increase in the maximum CFFT pile moment was obtained by increasing the FRP thickness from 5 to 9 mm. The maximum shear along the length of the composite pile was not noticeably

affected by the change in thickness. Therefore, in the parametric study the effect of FRP thickness was not found to be significant with regard to CFFT pile mechanical properties.

Effect of concrete strength

To evaluate the effect of concrete strength on the maximum lateral deflection, maximum moment, maximum lateral soil compressive stress, and maximum axial FRP stress, six different concrete strength values, ranging from 0 to 55 MPa, were used with lateral loads of 12, 50 and 100 kN. The corresponding graphs are presented in Fig. 7. With a lateral load of 100 kN, for concrete strengths of 30, 40 and 50 MPa, the maximum CFFT pile lateral deflections at the soil surface were found to be 32.7, 29.5 and 27.3 cm, respectively. Increasing the concrete strength from 25 to 55 MPa decreased the maximum axial FRP stress and the maximum moment by 14% to 15% and resulted in a five percent reduction in the maximum lateral compressive soil stress. It should be noted that the effect of different concrete strengths is more noticeable in the graphs than that of FRP thickness.

The small degree of influence may be due to the fact that elastic properties were mainly affected, and the plastic properties of concrete were not the primary factor in controlling the results. It should be mentioned that in most cases concrete strengths less than 25 MPa were not used, because these resulted in rupturing of the FRP tube. Hence, the effects of concrete strengths less than 25 MPa were investigated only under a small lateral load of 12 kN, as illustrated in Fig. 7. For a lateral load of 100 kN, with greater concrete strengths, the maximum lateral CFFT pile deflection was reduced by approximately 18%, while the maximum FRP and soil stress decreased by approximately 20%. In Fig. 7 (b), in the 100 kN curve the maximum moment exhibits a reduction of almost ten percent.

Effect of surrounding soil

The effect of soil type was investigated by using the numerical results for three different soil types, as shown in Fig. 8. The elastic moduli of the loose, medium, and dense sand used in this parametric study were 10, 30, and 60 MPa, respectively. The friction angle (φ) values related to the Mohr-Coulomb failure criterion were 32°, 36°, and 40° for loose, medium, and dense sand, respectively. As shown in Fig. 8 (a), the maximum lateral deflections of loose, medium, and dense sand were 26.9, 29.5, and 32 cm, respectively. As can be seen in Fig. 8 (b), denser surrounding soil decreased the maximum FRP axial stress by 17.4%. Similarly, the maximum moment was reduced by approximately 17%, as shown in Fig. 8 (d). Fig. 8 (c) shows that the maximum soil stress decreased by approximately 7%. Furthermore, the shear and axial load were reduced by nearly 6% to 8%, as seen in Fig. 8 (e) and (f). Thus, it can be concluded the effect of soil type is more noticeable than that of other parameters such as concrete strength, FRP thickness and pile diameter. Cohesionless soil such as sand collapses and flows with the composite pile upon reaching an active state, as the pile is laterally loaded. Thus, the gap in the interface is negligible in comparison to the pile displacement. Likewise, the change in soil stress during pile driving is negligible in comparison to changes in soil stress due to lateral loading of the composite pile (Achmus et al. 2009). For this reason, the effect of pile installation is ignored in the model.

Effect of load eccentricity

To obtain the normalized form of load eccentricity from the soil surface, the ratio of the height of the pile above the ground (h) to the embedded length of the pile in the soil (L_S) was considered to be the load eccentricity (e), as shown in Fig. 9. The effect of the applied load eccentricity (e) on

the maximum lateral deflection, maximum moment, maximum lateral soil stress, and maximum axial FRP stress was investigated. The results are presented in Fig. 10. It can be seen that increasing the load eccentricity from 0 to 0.3 results in a much greater increase in maximum lateral deflection and maximum moment for a lateral load of 100 kN, than for a lateral load of 12 kN. However, a lower rate of increase is seen in the maximum lateral soil stress and maximum axial FRP stress, due to the fact that the greater the height of the pile above ground level, the more FRP local buckling occurs in the pile. Thus, for lower values of load eccentricity, as illustrated in Fig. 10, increases in lateral load have a noticeable effect on the results; however, as higher load eccentricity values are reached, with greater above-ground pile lengths, failure is controlled by local buckling.

Local buckling of hollow FRP pile

Introducing the FRP tube values obtained by Fam et al. (2003b) into Eq. 7 yields $\sigma_{z,cr}$=161.4 MPa, which is greater than σ_z=120.2 MPa at the ground surface. In this case, local buckling at ground level is not the controlling factor for hollow FRP tube or CFFT pile failure. However, introducing the pile values into Eq. 8 yields $\sigma_{\theta,cr}$=1.29 MPa, whereas based on the values shown in the graphs σ_θ=27.81 kPa. In this case, local buckling will control failure under combined loading at the level of maximum FRP stress. This can be estimated by using Eq. 9, as follows:

$$C_{z\theta} = \left(\frac{\sigma_z}{\sigma_{z,cr}}\right)^2 + \left(\frac{\sigma_\theta}{\sigma_{\theta,cr}}\right)^2 = 1.49 > 1 \quad (13)$$

Table 2 shows local buckling factor ($C_{z\theta}$) values corresponding to different L/D ratios and FRP thicknesses (t). It can be seen that a pile with L/D=15 is very susceptible to local buckling, whereas FRP tubes with L/D=25 or a wall thickness of 9 mm are not subject to buckling. It should be noted that these values are overestimated for pure bending since not all of the cross-section is under

maximum compression. Furthermore, adding a low-strength internal material such as concrete with aggregates partially replaced by tire-derived aggregates (TDA) may prevent local pile buckling, providing a cost-effective and environment-friendly solution. Further research is needed to investigate the local buckling of FRP piles filled with other low-strength materials in addition to concrete.

Conclusion

In this research, a novel numerical model was developed to predict the behavior of concrete-filled FRP tube (CFFT) piles interacting with a soil foundation under lateral loading conditions. The model, based on nonlinear finite element analysis (NFEA) and the disturbed state concept (DSC), is a damage model that considers material and geometrical nonlinearity in addition to the interface of soil and FRP. A case study of a highway bridge on route 40 in Virginia was used to verify the model. Furthermore, a comprehensive parametric study was conducted to investigate the effect on CFFT pile behavior of the pile length to diameter ratio, FRP thickness, concrete strength, and soil strength. Different concrete strengths, including 32, 41, and 55 MPa, were considered with100 kN lateral loading. To examine the behavior of a hollow tube (having zero concrete strength) without failure, a 10 kN horizontal load was applied to the pile. The following conclusions can be drawn from this research:

- The slenderness of CFFT piles has a significant effect on their mechanical behavior. For example, decreasing the L/D ratio from 25 to 15 resulted in an 18% increase in the maximum moment.

- FRP thickness was found to be the least significant parameter in the parametric study. For instance, increasing the thickness from 5 to 9 mm resulted in only a five percent increase in the maximum moment of a CFFT pile.
- With a lateral load of 100 kN, decreasing the concrete strength from 55 to 25 MPa resulted in a 15% increase in the maximum moment of a CFFT pile. Furthermore, with an applied load of 10 kN, a 10% increase in the maximum moment was obtained by reducing the concrete strength from 20 to 0 MPa.
- In a parametric study of surrounding soil, dense sand with a friction angle of 40° resulted in a maximum moment 17% greater than that found for loose sand with a friction angle of 32°.
- Local buckling is a major controlling factor for FRP tubes at the maximum FRP stress level rather than at the ground surface. To address this issue, a low-strength internal material could be used to prevent local buckling of the pile.

Acknowledgments

The authors wish to acknowledge the Natural Sciences and Engineering Research Council of Canada for providing financial support.

Data Availability

All data, models, and code generated or used during the study appear in the submitted article.

References

Achmus, M., Kuo, Y.-S., and Abdel-Rahman, K. (2009). “Behavior of monopile foundations under cyclic lateral load.” *Computers and Geotechnics*, Elsevier, 36(5), 725–735.

ACI committee 318. (2014). “Building Code Requirements for Structural Concrete and Commentary.” *American Concrete Institute, Farmington Hills, MI*, 520.

Batdorf, S. B. (1947). “A simplified method of elastic-stability analysis for thin cylindrical shells.” *National Advisory Committee for Aeronautics*. Technical Note #1342, Langley Memorial Aeronautical Laboratory Langley Field, VA, USA.

Bowles. J.E. (1997), " Foundation analysis and design". 5th Edition, McGraw-Hill, New York, New York, United States.

Canadian Geotechnical Society (2006). *Canadian foundation engineering manual. 4th Edition, BiTech Publishers Ltd. Richmond, BC, Canada.*

Chae, K. S., Ugai, K., and Wakai, A. (2004). “Lateral resistance of short single piles and pile groups located near slopes.” *International Journal of Geomechanics*, American Society of Civil Engineers, 4(2), 93–103.

Desai, C. S. (2001). *Mechanics of Materials and Interfaces: The Disturbed State Concept*. CRC Press.

Desai, C. S. (2015). “Constitutive modeling of materials and contacts using the disturbed state concept: Part 1 – Background and analysis.” *Computers & Structures*, 146, 214–233.

Fam, A., Flisak, B., and Rizkalla, S. (2003a). “Experimental and analytical modeling of concrete-filled FRP tubes subjected to combined bending and axial loads.” *ACI Struct. J*, 100(4), 499–509.

Fam, A., Pando, M., Filz, G., and Rizkalla, S. (2003b). “Precast piles for Route 40 bridge in Virginia using concrete filled FRP tubes.” *PCI journal*, PRESTRESSED CONCRETE INSTITUTE, 48(3), 32–45.

Fam, A., and Rizkalla, S. (2001a). “Behavior of axially loaded concrete-filled circular FRP tubes.” *ACI Structural Journal*, 98(3), 280–289.

Fam, A. Z., and Rizkalla, S. H. (2001b). “Confinement Model for Axially Loaded Concrete Confined by Circular Fiber-Reinforced Polymer Tubes.” *ACI Structural Journal*, 98(4).

Giraldo Valez, J., and Rayhani, M. T. (2017). “Axial and lateral load transfer of fibre-reinforced polymer (FRP) piles in soft clay.” *International Journal of Geotechnical Engineering*, Taylor & Francis, 11(2), 149–155.

Han, F., Prezzi, M., and Salgado, R. (2017). “Energy-Based Solutions for Nondisplacement Piles Subjected to Lateral Loads.” *International Journal of Geomechanics*, 17(11), 04017104.

Hazzar, L., Hussien, M. N., and Karray, M. (2017). “Vertical load effects on the lateral response of piles in layered media.” *International Journal of Geomechanics*, 22(9), 1–11.

Helmi, K., Fam, A., and Mufti, A. (2005). “Field installation, splicing, and flexural testing of hybrid FRP/concrete piles.” *Special Publication*, 230, 1103–1120.

Liang, F., Chen, H., and Guo, W. D. (2013a). “Simplified boundary element method for kinematic response of single piles in two-layer soil.” *Journal of Applied Mathematics*, Hindawi, 2013.

Liang, F., Yu, F., and Han, J. (2013b). “A simplified analytical method for response of an axially loaded pile group subjected to lateral soil movement.” *KSCE Journal of Civil Engineering*, Springer, 17(2), 368–376.

Kulhawy, F. H., & Mayne, P. W. (1990). Manual on estimating soil properties for foundation design (No. EPRI-EL-6800). Electric Power Research Inst., Palo Alto, CA (USA); Cornell Univ., Ithaca, NY (USA). Geotechnical Engineering Group.

Mirmiran, A., and Shahawy, M. (1996). “A new concrete-filled hollow FRP composite column.” *Composites part B: engineering*, Elsevier, 27(3–4), 263–268.

Mirmiran, A., and Shahawy, M. (1997). “Behavior of concrete columns confined by fiber composites.” *Journal of structural engineering*, American Society of Civil Engineers, 123(5), 583–590.

Odland, J. (1978). “Buckling resistance of unstiffened and stiffened circular cylindrical shell structures.” *Norwegian Maritime Research*, 6(3).

Pando, M. A., Ealy, C. D., Filz, G. M., Lesko, J. J., & Hoppe, E. J. (2006). "A laboratory and field study of composite piles for bridge substructures (No. FHWA-HRT-04-043)." *United States. Federal Highway Administration. Office of Infrastructure Research and Development.*

Poulos, H. G. (2014). “Challenges in the design of tall building foundations.” *Geotechnical Engineering*, 45(4), 108–113.

Roddenberry, M., Mtenga, P., and Joshi, K. (2014). “Investigation of Carbon Fiber Composite Cables (CFCC) in Prestressed Concrete Piles.”

Schmertmann, J. H. (1975). "Measurement of in situ shear strength," *SOA Report. In Proceedings, ASCE Spec. Conference on In Situ Measurement of Soil Properties, Raleigh, NC, 1975* (Vol. 2, pp. 57-138).

Su, D., and Zhou, Y. G. (2015). “Effect of Loading Direction on the Response of Laterally Loaded Pile Groups in Sand.” *International Journal of Geomechanics*, 16(2), 4015051.

Zhang, L., Zhao, M., and Zou, X. (2013). “Behavior of laterally loaded piles in multilayered soils.” *International Journal of Geomechanics*, American Society of Civil Engineers, 15(2),

6014017.

Zhao, J. (2000). “Applicability of Mohr–Coulomb and Hoek–Brown strength criteria to the dynamic strength of brittle rock.” *International Journal of Rock Mechanics and Mining Sciences*, Elsevier, 37(7), 1115–1121.

Zienkiewicz, O. C., and Taylor, R. L. (2005). *The finite element method for solid and structural mechanics*. Butterworth-heinemann.

Table 1. Mechanical parameters used in the proposed model.

	Parameter	Concrete	Soil				FRP
			Sand 1	Sand 2	Sand 3	Clay	
Elasticity	E (MPa)	30,241	9.32	15.20	18.12	8.15	15,162
	ν	0.2	0.29	0.29	0.29	0.3	0.32
Plasticity	c (MPa)	6.43	0.1	0.1	0.1	5.0	-
	ϕ (deg)	55.51	34.0	38.0	42.0	29.0	-

Table 2. Local buckling factor ($C_{z\theta}$) values corresponding to different L/D ratios and FRP thicknesses (t).

Depth	L/D			t (mm)		
	15	20	25	5	7	9
Ground level	1.5	0.7	0.4	0.7	0.4	0.2
Maximum FRP stress	4.0	1.9	1.1	1.9	1.0	0.7

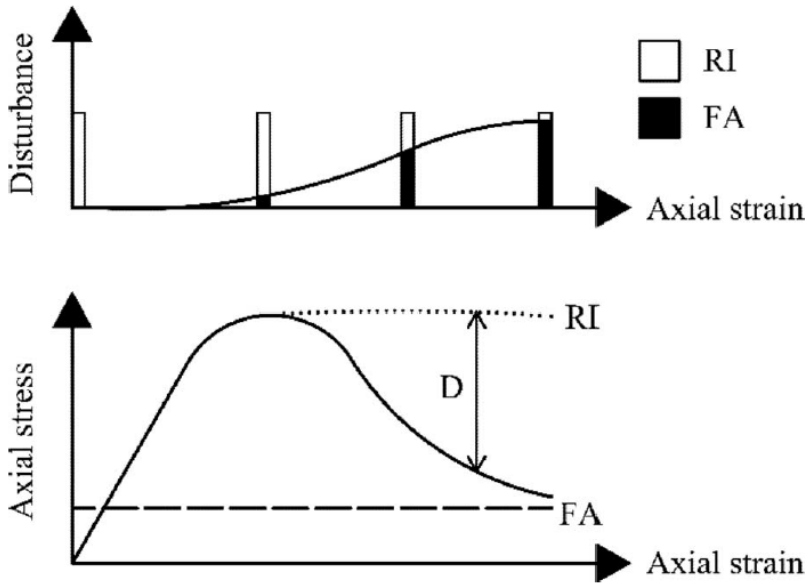

Fig 1. Schematic representation of DSC damage model based on the concept by Desai (2001)

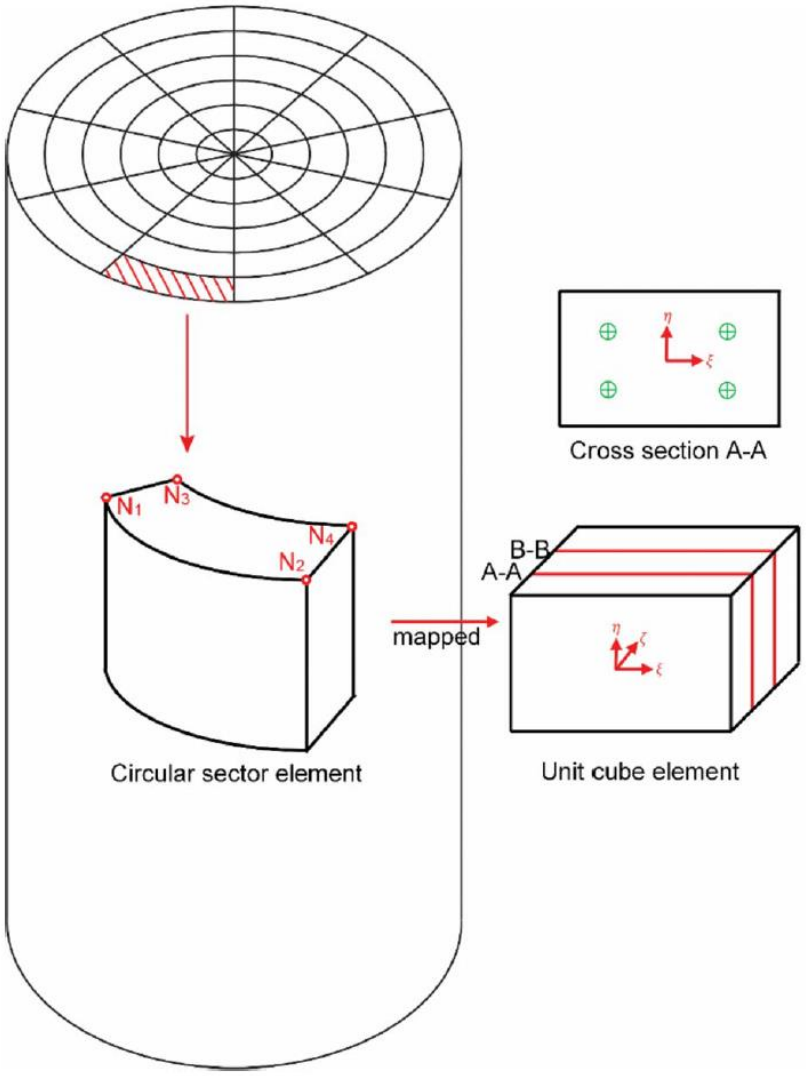

Fig. 2. Schematic configuration of mesh generated in a horizontal direction and mapping procedure used for quadratic interpolation and extrapolation of NFEA in three dimensions by considering eight Gaussian points

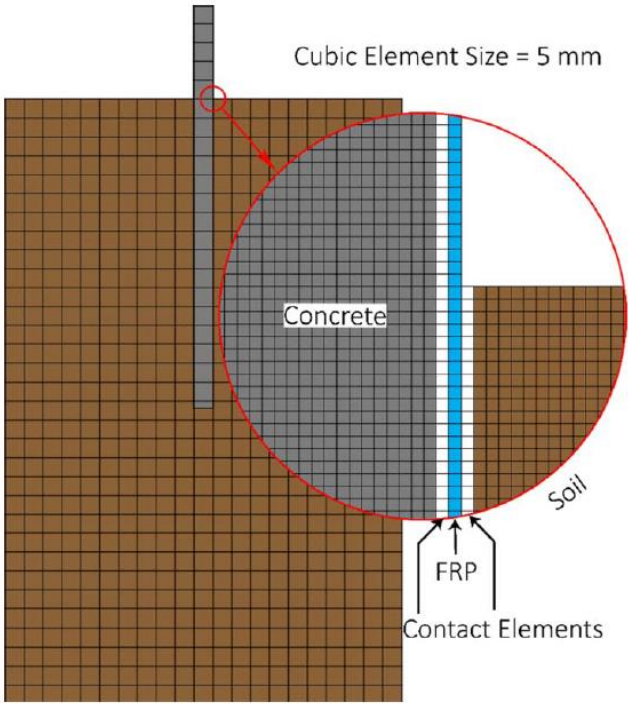

Fig. 3. Schematic representation of mesh generated for the interface of concrete, FRP laminate and soil in the proposed model

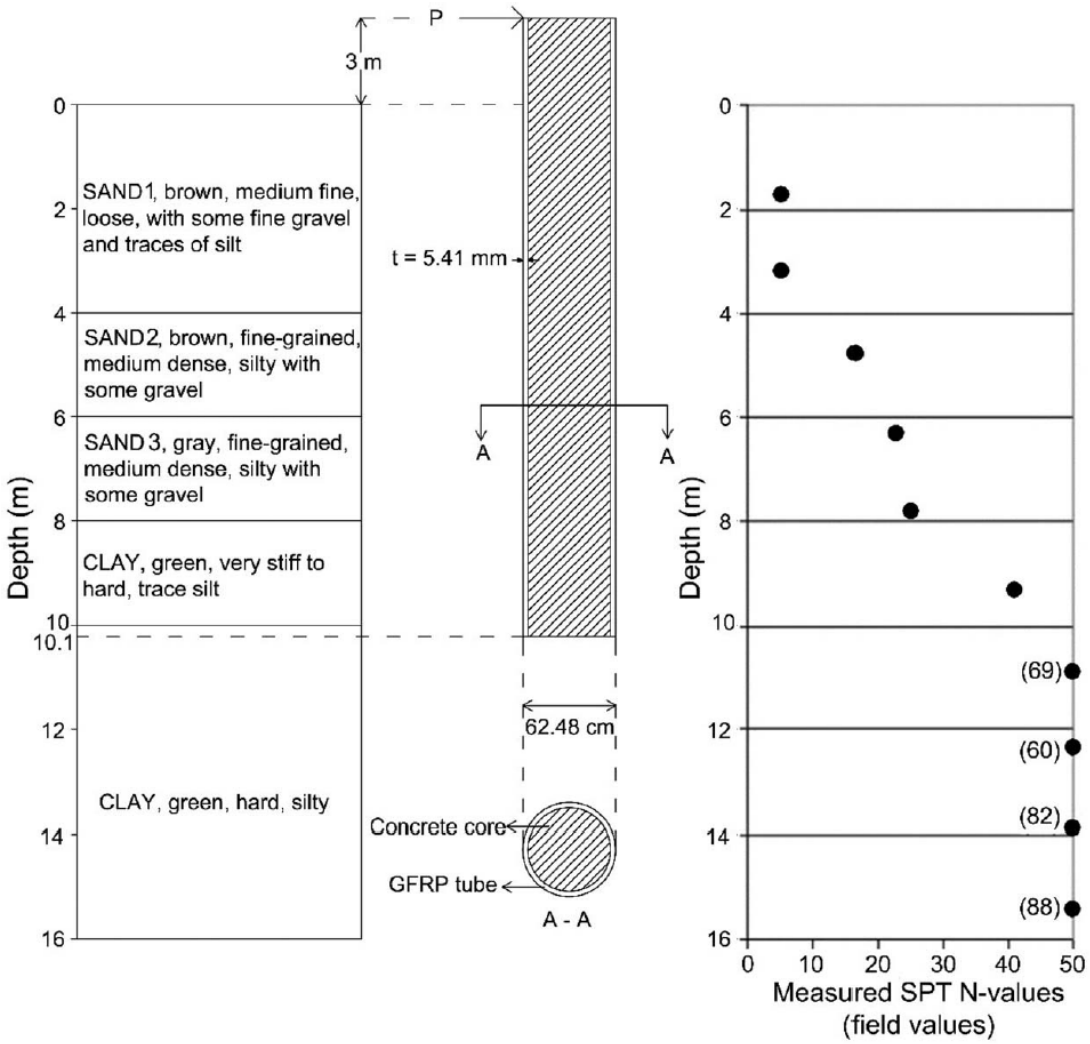

Fig. 4. Soil layers at different depths and composite pile profile (Fam et al. 2003b)

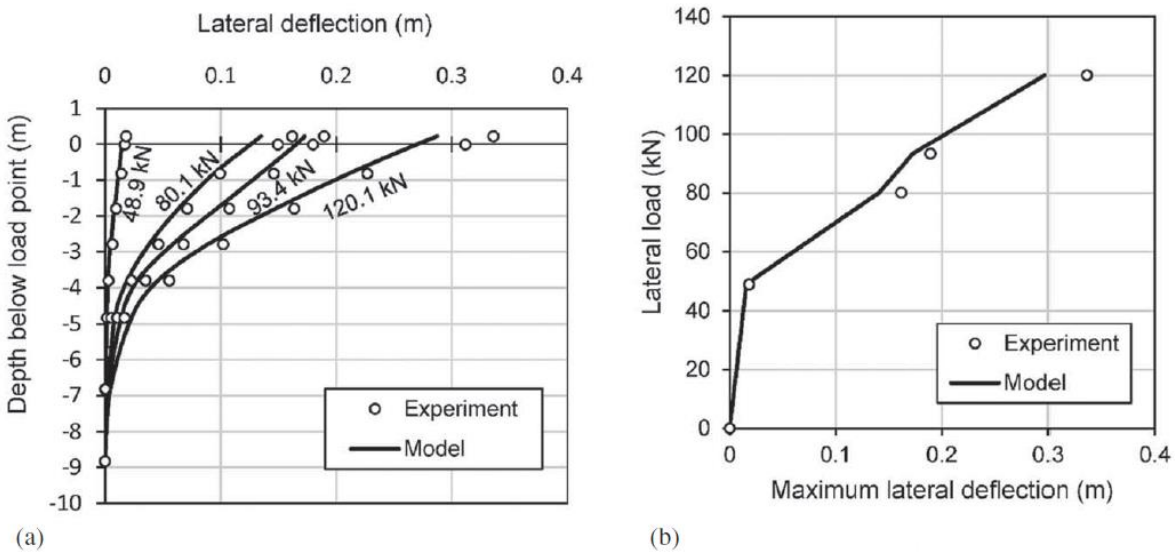

Fig. 5. Verification of the model against field data for lateral deflection along the length of a CFFT pile tested by Fam et al. (2003b) at different lateral load levels ranging from 48.9 to 120.1 kN

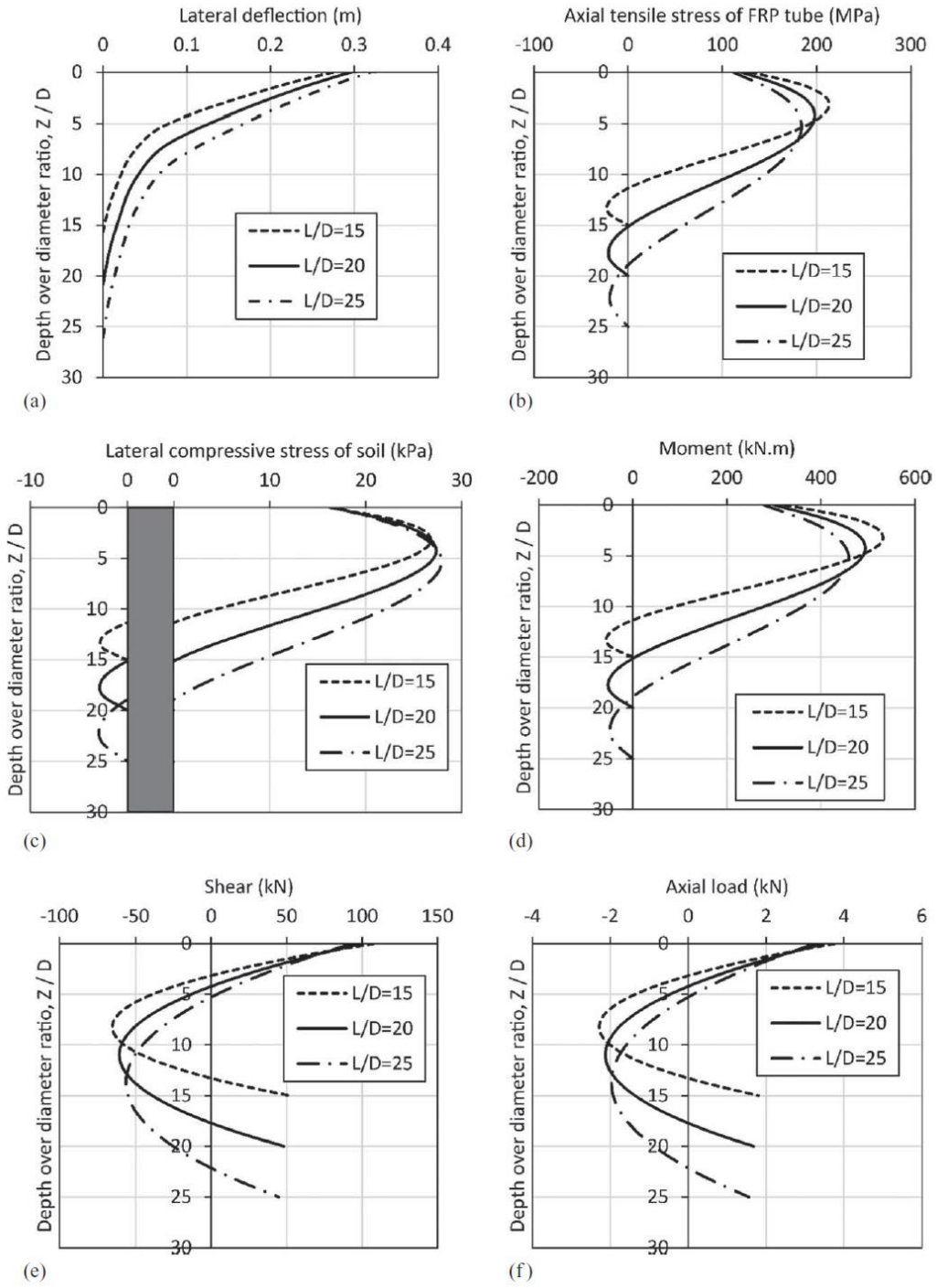

Fig. 6. Effect of the length/diameter (L/D) ratio on CFFT pile behavior, with a lateral load of 100 kN: (a) lateral deflection, (b) FRP axial tensile stress at the extreme tension fiber, (c) soil compressive stress, (d) bending moment, (e) shear force, and (f) axial load

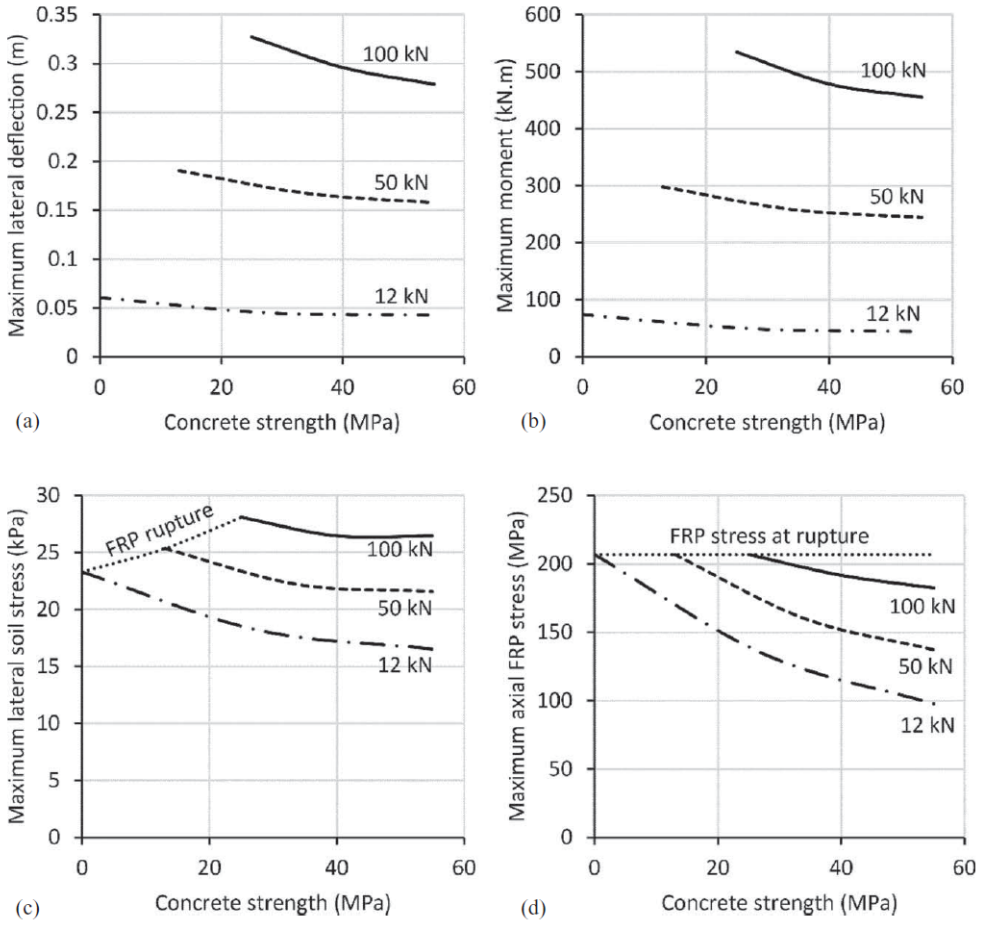

Fig. 7. Effect of the concrete strength on: (a) maximum lateral deflection, (b) maximum moment, (c) maximum lateral soil stress, and (d) maximum axial FRP stress of the CFFT pile, with lateral loads of 12, 50 and 100 kN

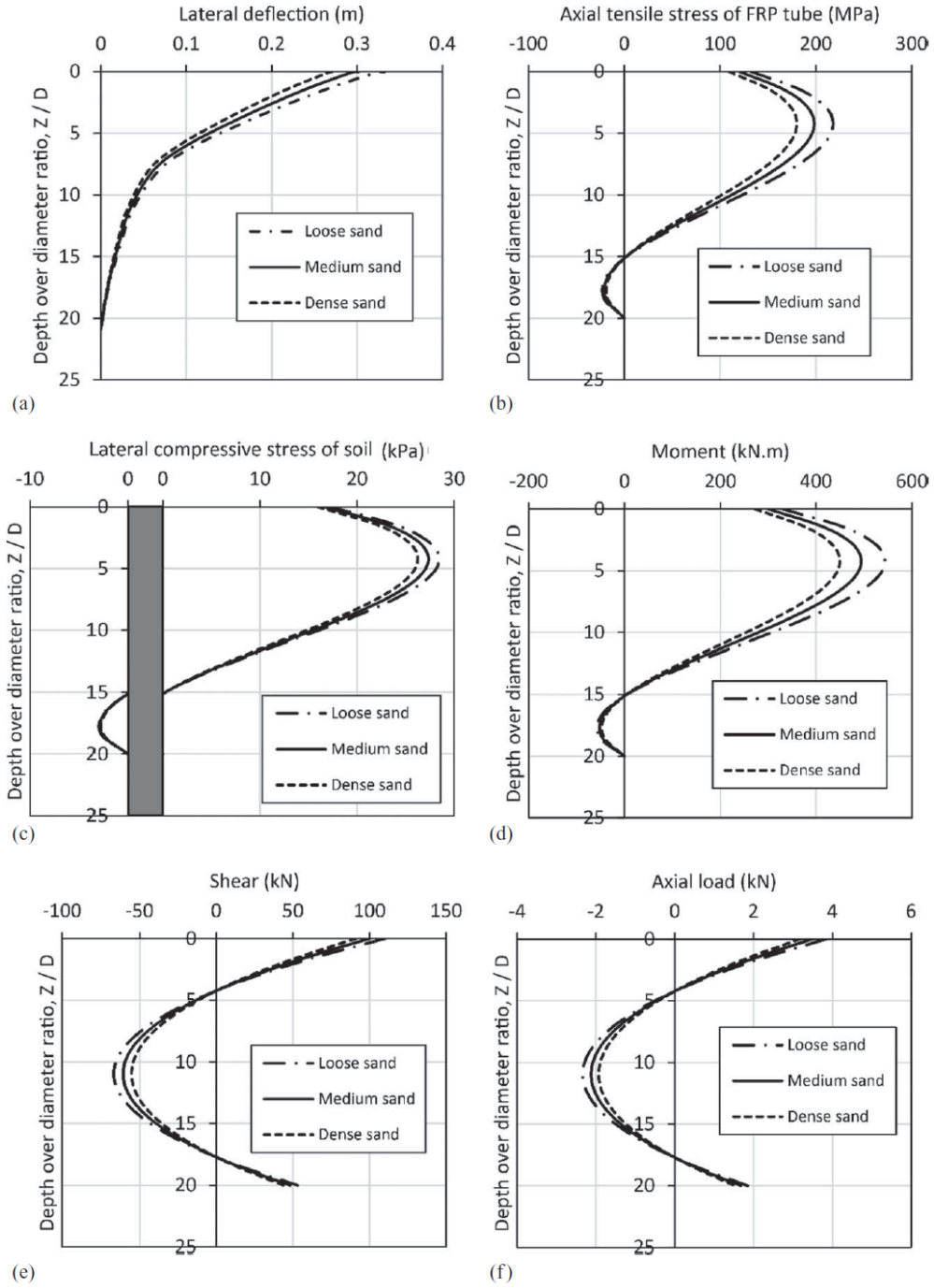

Fig. 8. Effect of the soil type on CFFT pile behavior, with a lateral load of 100 kN: (a) lateral deflection, (b) FRP axial tensile stress at the extreme tension fiber, (c) soil compressive stress, (d) bending moment, (e) shear force, and (f) axial load

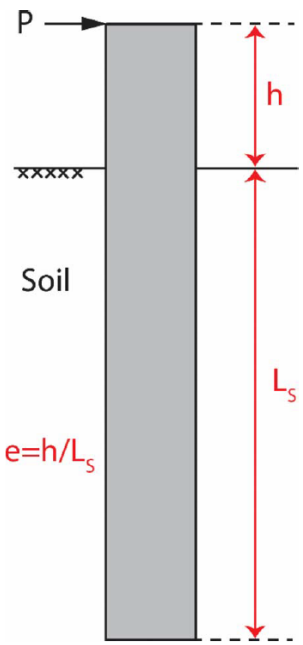

Fig. 9. Applied load eccentricity (e) with respect to embedded length of the pile in the soil (L_S)

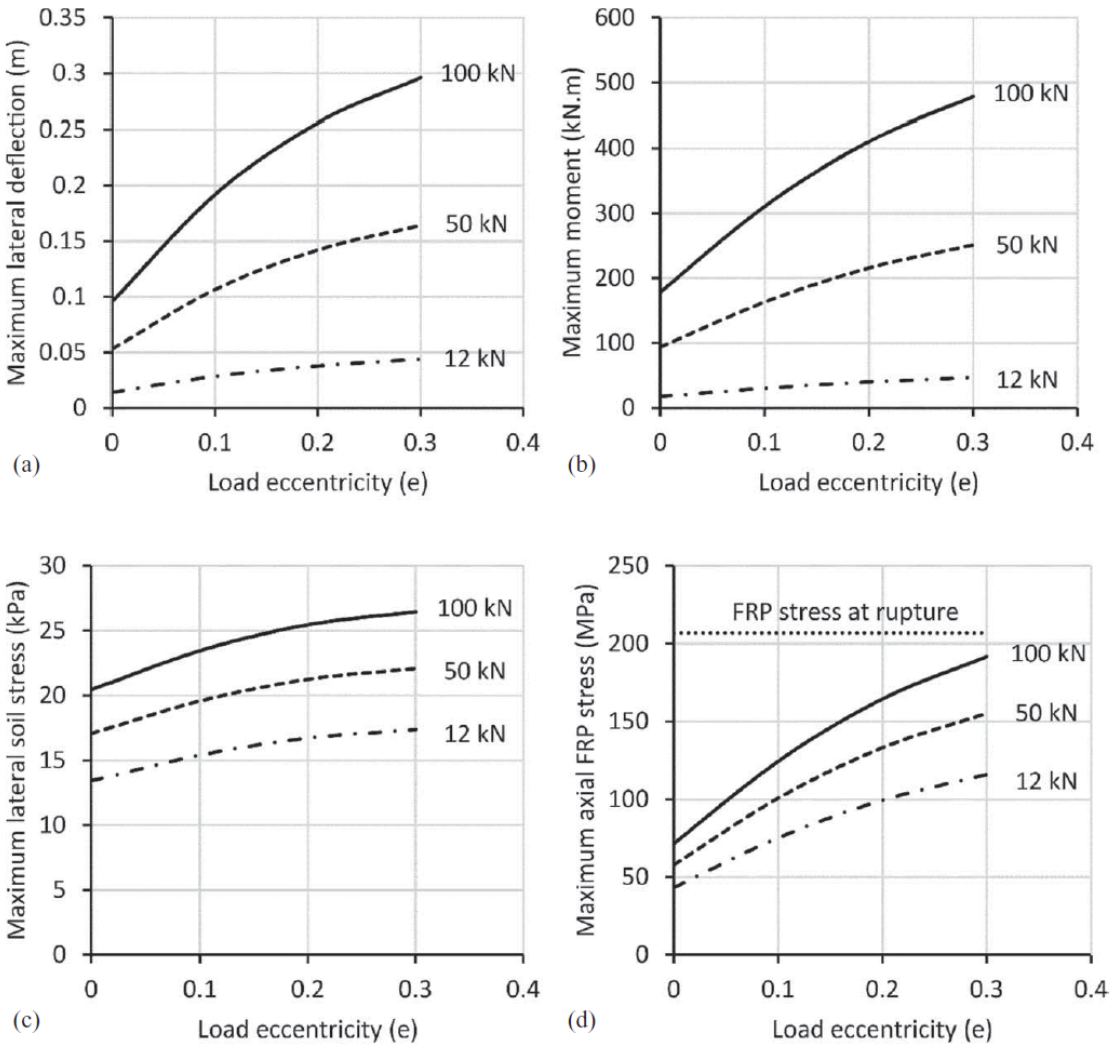

Fig. 10. Effect of the normalized load eccentricity (e) on: (a) maximum lateral deflection, (b) maximum moment, (c) maximum lateral soil stress, and (d) maximum axial FRP stress of the CFFT pile, with lateral loads of 12, 50 and 100 kN